JOURNAL OF Materials CHEMISTRY

Thickness control and defects in oriented mesoporous silica films

Hong Yang, Neil Coombs and Geoffrey A. Ozin*

Materials Chemistry Research Group, Lash Miller Chemical Laboratories, University of Toronto, 80 St. George Street, Toronto, Ontario, Canada, M5S 3H6

By using a surfactant-based synthesis strategy, we have earlier demonstrated that the polymerization and growth of silicate micellar assemblies at the air–water interface, under quiescent and dilute acidic aqueous conditions, yields free-standing submicron thickness hexagonal mesoporous silica films in which the channels are oriented parallel to the film surface. TEM imaging studies of these thin films showed that microscopic defects pervade the channel structure with topologies resembling those found in lyotropic liquid crystals. This suggested that the mesoporous silica film evolved from silicification of a surface lyotropic silicate mesophase. Herein it is demonstrated that film growth, defect structure, extent of polymerization, and mesoporosity sensitively depend on the choice of synthesis acidity, temperature and mixing, and in the case of supported films, on the choice of substrate. In particular, a ten-fold increase in the thickness of the film can be obtained by simply lowering the acidity and moving to ambient temperature conditions whilst an alteration in mixing conditions can change the film from a discrete to a continuous morphology. Combined PXRD, TEM and nitrogen adsorption studies show that the silica films are hexagonal, oriented and mesoporous. Furthermore, the observation of a focal conic fan-type texture in the free-standing films shows that defect controlled director fields, that exist in a precursor hexagonal lyotropic silicate mesophase, are preserved in the channel structure of the mesoporous silica phase. Proof-of-existence of liquid crystalline texture in such free-standing mesoporous silica films, provides direct evidence that film growth evolves from the cooperative assembly and organization of silicate micellar species at the air–water interface.

Introduction

Liquid crystals represent a delicate phase of matter which has lost long range positional order of ordinary crystals but retains orientational order of anisotropic structural units.[1–3] Defects in liquid crystals, unlike their atomic scale counterparts in normal crystals, are microscopic in size, their formation requires much less energy, and their topology determines the patterns of director fields. They are responsible for birefringence textures made visible between cross polarizers in an optical microscope where distinct patterns are diagnostic of particular liquid crystal structure types.[2,3]

In this context, it has recently been demonstrated that the polymerization of silicate micellar assemblies[4,5] at the air–water interface, under dilute and acidic aqueous conditions, yields free-standing hexagonal mesoporous silica films with a thickness of *ca.* 0.5 μm, in which the channels are oriented parallel to the film surface.[6–9] Free-standing hexagonal mesoporous silica films with a different space group, $P6_3/mmc$, were subsequently reported.[10] Herring bone, U-shaped and S-shaped channel designs have been observed by TEM in these hexagonal mesoporous thin film samples.[7] Their channel architecture[6–8] displayed a close resemblance to the director field patterns in hexagonal organic liquid crystals that are usually associated with common line defects,[11–13] such as $+\pi$, $-\pi$ disclinations, pairs of $+\pi$ disclinations, edge dislocations, bending and wall defects.[14]

In this article we show that by simply employing less acidic synthesis conditions than those in our earlier study, it is possible to realize at least a ten-fold increase in the thickness of the mesoporous silica films, while mixing conditions can also affect the morphology of the films. Polarizing optical microscopy shows that these thick films display a fan-type texture diagnostic of a hexagonal lyotropic organic liquid crystal, H_I phase. Significantly, the texture is maintained on removing the surfactant and after thermally annealing the films. This implies that the optical birefringence emerges from the polarization response of electron density circumscribing a hexagonal array of mesoscale glassy channels, that is, 'mesoscale optical anisotropy in glass'.[15]

It is worth mentioning that while different surfactant-based templating strategies have been successfully used to synthesize mesostructured materials, the formation pathways are not necessarily the same.[4,5,8,16–22] In the concentrated surfactant regime, the formation of mesostructured materials likely proceeds through the mineralization of a pre-existing liquid crystal mesophase.[21] By contrast, in the dilute regime, the mesostructure likely forms by mineralization of a co-assembly of silicate micellar templates.[4,5,16–18] In this study, proof-of-existence of hexagonal liquid crystalline texture in free-standing mesoporous silica films that are grown at the boundary between air and water under very dilute aqueous conditions, provides evidence that film growth occurs through the cooperative assembly pathway.

Experimental

Synthesis

The film synthesis procedure involved a modified version of that reported earlier for the preparation of mesoporous silica morphologies.[7,15] Tetraethylorthosilicate (TEOS, 99.999+%, Aldrich), cetyltrimethylammonium chloride (CTACl, 29 wt.% aqueous solution, Pflatz & Bauer) and hydrochloric acid (36.5–38 wt.% aqueous solution, BDH) were used as received. The reactant ratios used for making the film with a thickness of *ca.* 5–10 μm were 100 H_2O : 1.0 HCl : 0.11 CTACl : 0.13 TEOS. In a standard preparation, 2.9 g of a CTACl surfactant aqueous solution (29 wt.%) was mixed well with 2.5 g of HCl solution (36.5–38%) and 40.8 g of deionized water by using a magnetic stirrer (Corning PC-351 hot plate stirrer) with a 0.375 in × 1.5 in stir bar in a polypropylene beaker followed by adding 0.65 g of TEOS. The mixture was then stirred for 3 to 10 min at room temperature. The final mixture was transferred into either a round or a square polypropylene (PP) or low density polyethylene (LDPE) bottle with different diameters and length of edge (Nalgene®, LABCOR, Inc.), and allowed to achieve a quiescent state. The mesoporous silica growth process was typically allowed to proceed for a period of one week under static conditions at room temperature. Depending on the initial time period and the stirring rate for the mixing,

different optical birefringence textures were observed. The film on mica was grown by allowing a freshly cleaved muscovite mica substrate (J. B. EM. Services Inc., Dorval, Quebec) to float on the solution surface. The calcination of the film was achieved using two different procedures. Direct calcination was done in air and in a furnace attached to an Omega CN-2010 programmable temperature controller. The temperature ramp was less than 1 °C min^{-1} and typically the sample was held at 450 °C for 4–10 hours. The other calcination method involved two steps, the sample was first dehydrated at 150 °C for over 10 hours under $\leqslant 10^{-5}$ Torr dynamic vacuum and then heated in air at 450 °C for *ca.* 10 hours. Most of the characterization work for the as-synthesized and calcined film samples was done with those having a fan type texture and using the direct calcination procedure unless mentioned otherwise.

Characterization

Powder X-ray diffraction (PXRD) data were obtained on a Siemens D 5000 diffractometer using Ni-filtered Cu-Kα radiation with $\lambda = 1.54178$ Å. Home made quartz low background sample holders and plexiglass sample holders were used for mounting the intact films or ground films, and for recording the PXRD patterns. Scanning electron microscopy (SEM) images were obtained on a Hitachi S-4500 field emission microscope using a low acceleration voltage of 2 kV to minimize the charging of the mesoporous silica surfaces. Samples were uncoated and imaged directly. Transmission electron microscopy (TEM) images were recorded on a Philips 430 microscope operating at an accelerating voltage of 100 kV with a typical recording magnification in the range 80 000 to 160 000 times. The microscope has a working resolution of 3.5 Å. In order to get ultrathin (*ca.* 400–600 Å) sections of the mesoporous silica morphologies, the samples were embedded in epoxy resin and sectioned using an RMC MT6000 ultramicrotome in combination with a Drukker diamond knife following the standard procedure. Embedding in Spurr's epoxy resin (TAAB laboratories equipment, Aldermaston, UK) was used for calcined film samples and a cyanoacrylate resin (Superglue®) for as-synthesized film samples. Additional hardening of the embedding matrix was induced at 60 °C for 12 hours. Polarized optical microscopy (POM) images were obtained on a BH-2 Olympus optical microscope with a Kodak Gold Ultra 400 film. Proton-decoupled ^{29}Si solid state magic angle spinning nuclear magnetic resonance (MAS NMR) spectra were recorded on a Bruker DSX 200 MHz spectrometer at 40 MHz using a 90° pulse with a delay time of 600 seconds. Computer simulation of the NMR spectra employed a Bruker deconvolution program. Thermal analysis (DSC and TGA) data were recorded on Perkin-Elmer Thermal Analysis Series 7 instrumentation under N_2. The temperature ramp was at 5 °C min^{-1}. The surface area and mesoporosity of the film were obtained on a McBain balance. Details of the set-up and measurement procedure have been published elsewhere.[23] To prepare a sample for the measurement of adsorption isotherms, a sufficient quantity of the as-synthesized films was first ground to a fine powder and then calcined following either one of the calcination procedures mentioned above.

Results

An optical microscopy image of a free-standing film obtained in a synthesis that employed an agitation time of 10 minutes shows that the film is optically transparent. Scanning electron microscopy (SEM) images of the film are shown in Fig. 1. The film is continuous and the surface of the film that grows adjacent to the air interface has a smoother surface than that of the growing front emerging at the water interface, Fig. 1(A). The observed bending of the film presumably arises from a stress induced drying effect. A cross-sectional view of the film

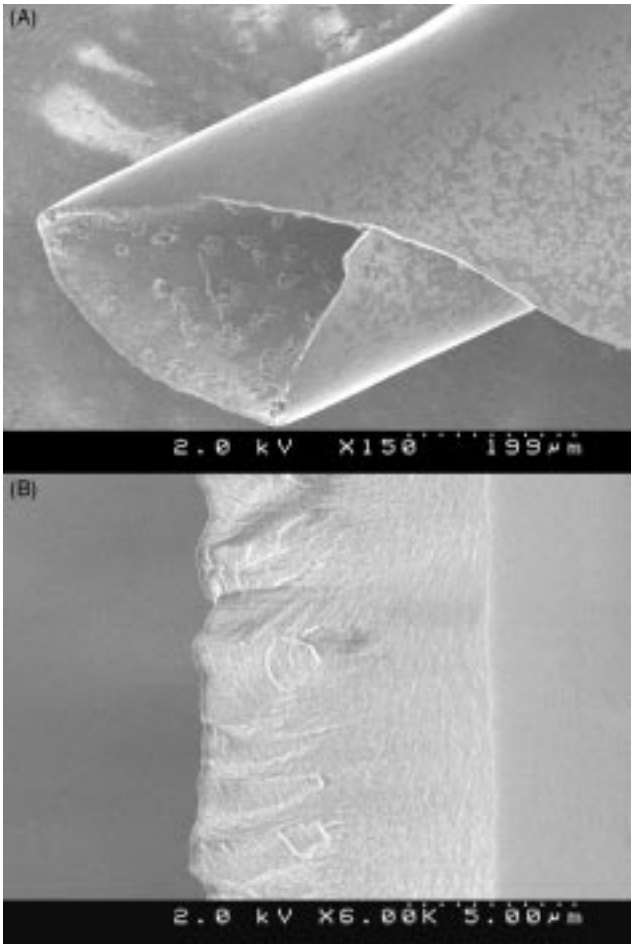

Fig. 1 Representative SEM images of an as-synthesized mesoporous silica film formed at the air–water interface showing (A) a typical surface with bending, and (B) cross section with a thickness of *ca.* 5–10 µm

shows the thickness to be *ca.* 5–10 µm thick, Fig. 1(B). The thickness of the film that grows at the air–water interface depends on the conditions of the solution phase. Representative POM images obtained between crossed polarizers, for mesoporous silica films formed under slightly different conditions are shown in Fig. 2. In contrast to the previously reported images for $\leqslant$*ca.* 0.5 µm mesoporous silica thin films,[6] the newly obtained thick films display classic liquid crystal textures. The transformation of the films from ones displaying discrete birefringent patterns, Fig. 2(A), to ones with fan-type textures, Fig. 2(B), can be controlled by simply choosing the stirring time or rate of the synthesis mixture before it is set into a quiescent growth state. The films that have a fan-type texture were obtained for the mixture with a stirring time of about 10 minutes at low stirring rate, Fig. 2(B), or about 5 minutes at high stirring rate, while the ones showing discrete birefringence patterns emerged after a stirring period of 3 to 5 minutes at low stirring rate, Fig. 2(A). The observed fan-type texture is typical of a hexagonal lyotropic liquid crystal H_I phase having the optical axis in the plane of the film.[2,3] The fan-type texture is essentially invariant on removing the surfactant and after annealing the film at 450 °C, Fig. 2(C). This implies that the optical birefringence of the film does not require the surfactant to be present in the channels and that strain anisotropy in the film is not the source of the fan-type texture. The study herewith was conducted with samples that have fan-type textures obtained for the mixture with a stirring time of about 10 minutes, at low stirring rate of the synthesis mixture before it is set into a quiescent growth state, unless stated otherwise.

Powder X-ray diffraction (PXRD) traces of these meso-

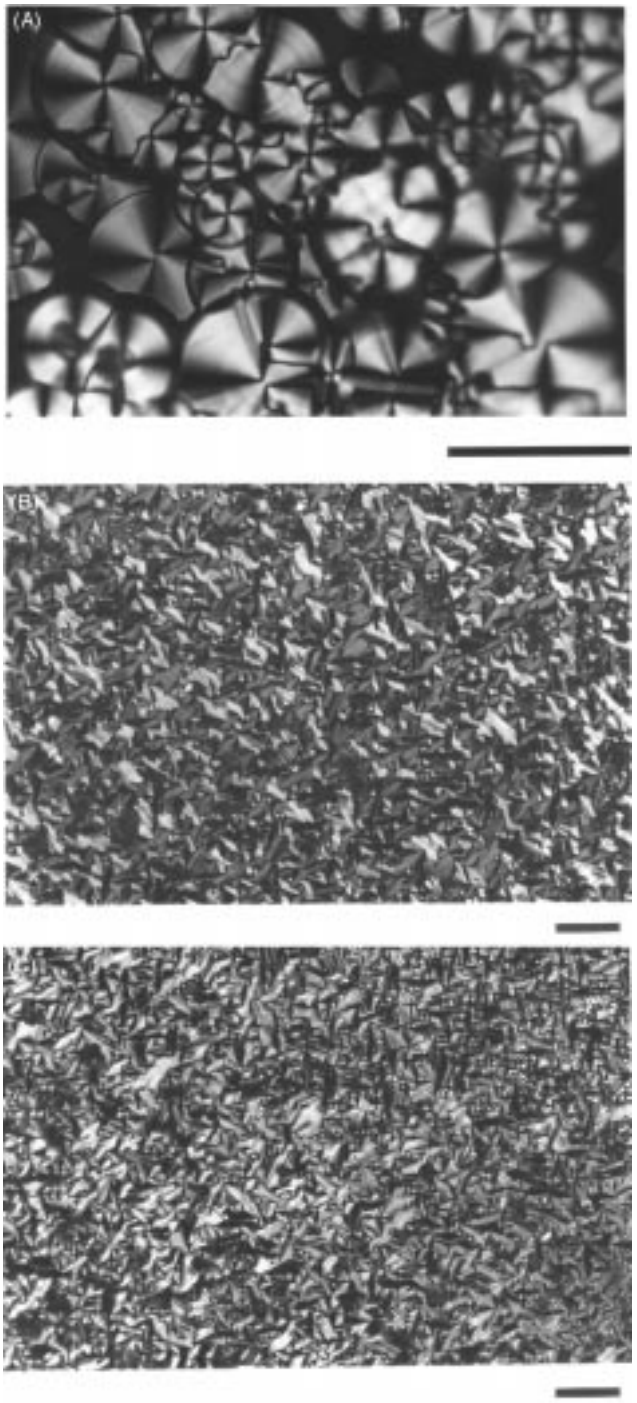

Fig. 2 POM images of mesoporous silica films under cross polarizers: (A) discrete texture of an as-synthesized film; fan-type texture of (B) an as-synthesized and (C) a calcined film (scale bar: 50 μm)

porous silica films are shown in Fig. 3. The PXRD pattern of as-synthesized and calcined film confirm them to be hexagonal mesoporous silica and not the silicate liquid crystal mesophase for which the d_{100} appears at much lower angles,[17] Fig. 3. The presence of only (100, 200) low angle reflections, Fig. 3(a), implies that the channels preferentially run parallel to the surface of the film.[6] This structure is retained after surfactant removal by calcination and is accompanied by contraction of the hexagonal mesostructure due to condensation–polymerization of residual hydroxyls in the silica channel walls.[4] The relatively large contraction of the d_{100} spacing for the calcined film, Fig. 3(c), implies a much lower degree of polymerization of the silica in the surfactant-containing precursor film relative to a higher acidity synthesis (see below).[6–9] The structure of

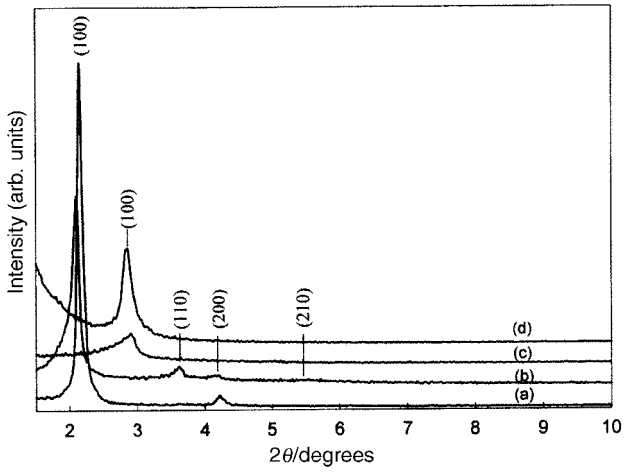

Fig. 3 PXRD traces of as synthesized mesoporous silica films, (a) without and (b) with grinding; calcined mesoporous silica films, (c) without and (d) with grinding

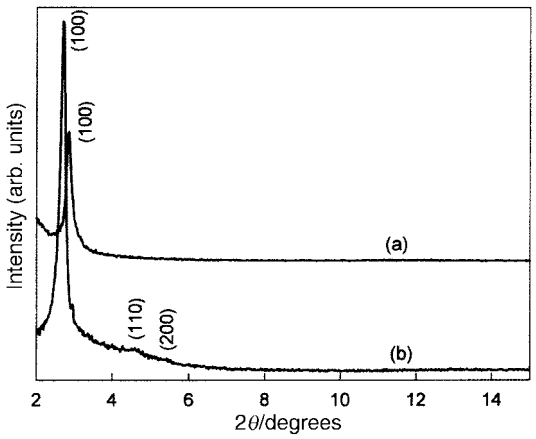

Fig. 4 PXRD traces of (a) calcined ground film without dehydration and (b) calcined ground mesoporous silica films after dehydration treatment

the oriented mesoporous films was investigated further by examining the effect of grinding. The ground-up film samples are white powders. The PXRD trace for the ground sample, Fig. 3(b), showed the expected four peaks (100), (110), (200), (210) from diffraction planes that are typically seen in randomly oriented powder preparations of hexagonal mesoporous silica.[4,5] The calcined and annealed ground-up samples, Fig. 3(d), also show a large contraction of the d_{100}-spacing similar to that for the calcined oriented film, Fig. 3(c). It is observed that after the vacuum dehydration treatment at 150 °C, the d_{100} diffraction peak contracts *ca.* 2 Å, and then further calcination of the dehydrated sample leads to a more well ordered mesoporous silica structure than that obtained without the vacuum pre-treatment. This is evidenced by a higher diffraction intensity and a greater number of reflections in the PXRD patterns of the pretreated samples, Fig. 4. Clearly the moisture content of an as-synthesized incompletely polymerized mesoporous film can affect the stability of the structure.[24]

The orientation of the channels for the as-synthesized and calcined hexagonal mesoporous films is confirmed by TEM images of microtomed thin sections, Fig. 5. The expected hexagonal honeycomb structure is seen in both as-synthesized and calcined mesoporous silica films. Careful inspection of the TEM images shows that the hexagonally packed pores are not as well organized as those in the thinner version of the film made at 80 °C. It is unlikely that such a difference is simply from the variation of imaging conditions. Note that a lower

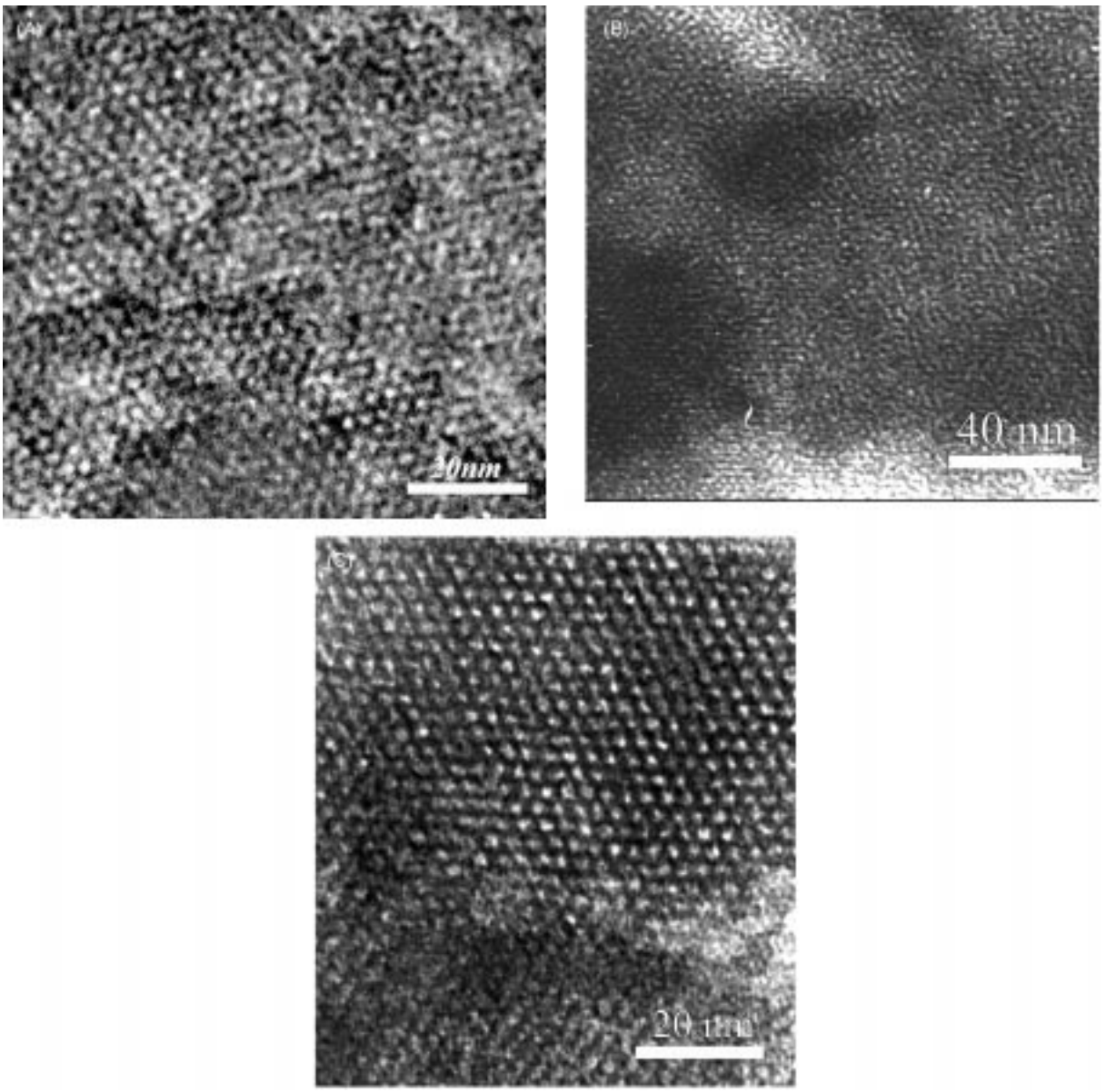

Fig. 5 Representative TEM images of mesoporous silica films: (a) as-synthesized, (b) calcined (no dehydration treatment), (c) calcined (with dehydration treatment)

degree of condensation–polymerization of silica (see below) may lead to a less stable channel wall structure for the embedding and microtoming procedure. As far as we can judge from the TEM images, the order of the mesopores on the top (air interface) and bottom (water interface) faces of the films is about the same. Vacuum dehydration prior to calcination seems to be an essential step for stablizing a well ordered hexagonal mesoporous structure. Calcination without vacuum dehydration appears to cause a greater distortion of the hexagonal mesoporous structure, Fig. 5(b).

Thermogravimetric analysis (TGA) of the as-synthesized film shows the expected weight changes corresponding to loss of imbibed water below 100 °C, surfactant template around 270 °C, and water from condensation of framework hydroxyls around 360 °C and 600 °C, Fig. 6. The total weight decrease is *ca.* 60–70% which represents a high-end loss for a hexagonal mesoporous silica preparation. This is presumably because of the lower degree of polymerization and larger amount of surfactant template imbibed within the channels.

Differential scanning calorimetry (DSC) shows no evidence of an endotherm that can be ascribed to a liquid crystal or isotropic liquid melting transition of the encapsulated surfactant for a heating cycle between 20 °C and 250 °C, Fig. 7. The

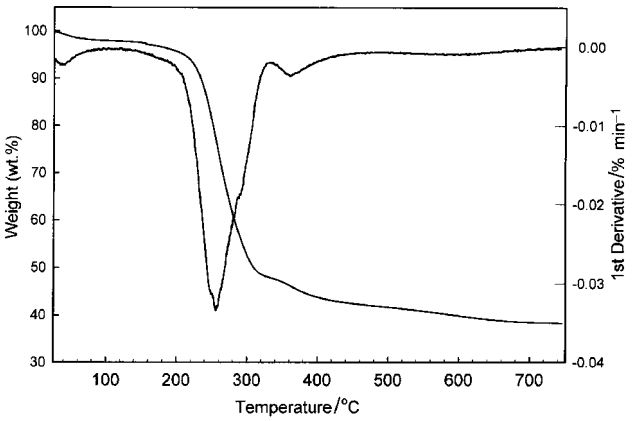

Fig. 6 A representative TGA trace of a mesoporous silica film

combined results of the TGA and DSC show that the thermal properties of these mesoporous silica films closely resemble those of the powdered solid. Moreover, the imbibed surfactant within the channels is not behaving like a liquid crystal mesophase.

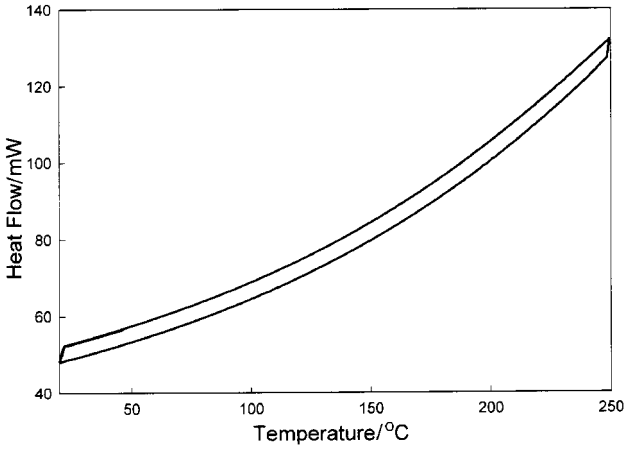

Fig. 7 A representative DSC trace of an as-synthesized mesoporous silica film with a heating cycle up to 250 °C

The proton-decoupled ^{29}Si MAS NMR spectrum and computer deconvolution of the spectrum for the as-synthesized mesoporous silica film are shown in Fig. 8. Three silicon sites are observed with a $Q_2[SiO_2(OH)_2]:Q_3[SiO_3(OH)]:Q_4(SiO_4)$ ratio of 8:42:48. The observation of Q_2 silicon species and the high value of Q_2+Q_3 relative to Q_4 are consistent with the observed large contraction of the hexagonal mesostructure on calcination (PXRD). This implies a lower degree of silicate polymerization in the as-synthesized thick films compared to the thin ones, as well as the usual mesoporous powders.

Quantification of the mesoporosity and surface area of the film was conducted on a McBain balance.[23] N_2 isotherms at liquid nitrogen temperature are shown in Fig. 9. The as-synthesized silica films show negligible N_2 adsorption after dehydration at 150 °C in vacuum implying that this treatment does not create void space for adsorbing N_2. The isotherm for the vacuum dehydrated–calcined sample is typical of that expected for Type IV demonstrating that the sample is mesoporous.[25] The BET surface area is calculated to be *ca.* 1000 m^2 g^{-1}. The mean pore diameter estimated by the Dollimore–Heal method from the adsorption branch of the isotherm is *ca.* 2.8 nm, which is consistent with the center-to-center distance of *ca.* 3.7 nm obtained from PXRD of calcined mesoporous film samples. Note that the desorption branch of the isotherm

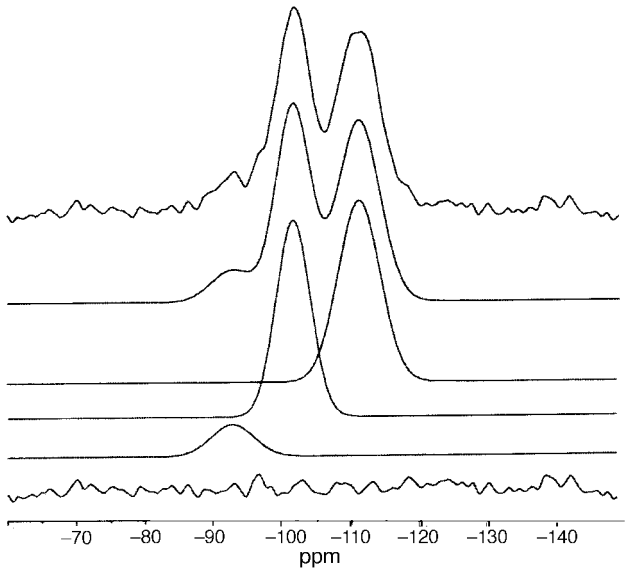

Fig. 8 The proton-decoupled ^{29}Si MAS NMR spectrum and computer deconvolution of the spectrum for the as-synthesized mesoporous silica film

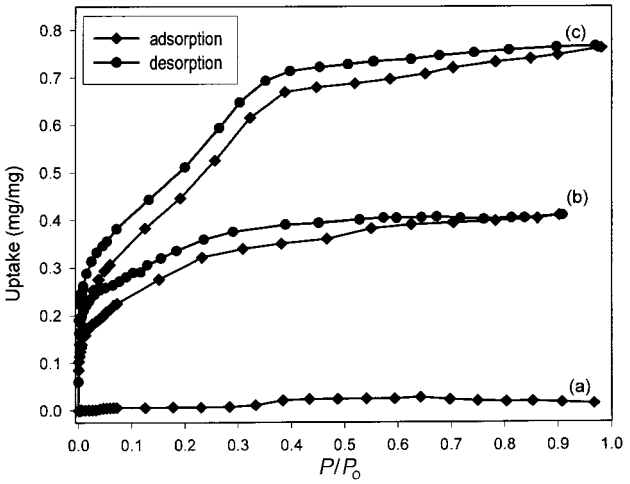

Fig. 9 Nitrogen isotherms of free-standing oriented mesoporous silica films: (a) sample after dehydration at 150 °C, (b) sample calcined without dehydration pre-treatment, and (c) sample calcined with dehydration pre-treatment. All samples were ground into a powder before the adsorption measurements

shows both low and high pressure hysteresis. It is well documented that particular shapes of hysteresis loops can be associated with specific pore structures.[25a] Low pressure hysteresis in this case may be associated with distortion swelling of the walls of a partially condensed mesoporous silica accompanying adsorption.[25a] The isotherm for the directly calcined sample shows a lower uptake of nitrogen, has a much shallower inflection due to capillary condensation, and also displays low and high pressure hysteresis. The BET surface area is calculated to be *ca.* 750 m^2 g^{-1}. These observations together with those from PXRD, TEM and NMR suggest that the vacuum-dehydration pre-treatment prior to calcination substantially improves the degree of order and mesoporosity of the silica films.

The thick mesoporous silica films can also be grown on a variety of substrates, such as glass slides and tubes, and freshly cleaved muscovite mica. For the preparation of these films, the 10 minute mixing period described above was used. Between crossed polarizers in the optical microscope, discrete birefringence patterns were observed for the films grown on planar and curved glass substrates. The discrete patterns on glass appear to arise from the local nucleation and growth of silicate-surfactant assemblies with contributions from $+2\pi$ disclination[12–14] concentric-type topological defects. Similar POM patterns have been observed for mesoporous silica discoid shapes that concurrently form in the bulk synthesis mixture.[15] Interesting birefringence patterns were observed for the thick

Fig. 10 A representative POM image of an as-synthesized mesoporous silica film on mica (image size is 150×120 μm)

films grown on freshly cleaved muscovite mica, Fig. 10. Light coloured, grey and dark areas were observed for the thick films between crossed polarizers.

Careful inspection of these images showed that striations on the patches with the same brightness align parallel on the film surface and that the lines on patches with differing brightness meet at 60° or 120° angles. Recall that oriented mesoporous silica films have been reported to grow on this surface.[26] Thus the observed correlation of striations amongst similarly coloured domains, Fig. 10, presumably originates from preferential alignment of the channels in the mesoporous silica film along the hexagonal *a*,*b*-axes of the mica surface.

Discussion

Quiescent, acidic and aqueous conditions are the key and essential prerequisites for our surfactant-templated synthesis of hexagonal mesoporous silica films at the boundary between air and water.[6,7] Under high acidity and 80 °C reaction conditions the films grow to a limiting thickness of about 0.5 μm. TEM images of the films show that while the channels are well organized in the plane of the film, they swirl and curl throughout the body of the film to create designs[7,8] that resemble the patterns of director fields induced by topological defects such as $+\pi$, $-\pi$ and $+2\pi$ disclinations found in a discotic hexagonal liquid crystal mesophase.[12,13]

Studies of the early stages of film growth suggest that the process begins with the assembly of silicate liquid crystal seeds located at the air–water interface and templated by a surfactant overstructure.[6,7,27–30] They silicify and expand in size through the accretion of silicate micelles and coalesce to form a continuous film. Concurrent with film growth in two dimensions, mesoporous silica morphologies with well defined three dimensional shapes are evolving in the bulk aqueous phase. The reactant ratios, temperature and acidity of the synthesis are important factors for controlling the curvature and size of these morphologies.[15] In particular, it was found that less acidic and room temperature conditions promoted the growth of well formed morphologies with dimensions as large as *ca.* 70 μm. With this knowledge of size and shape control of mesoporous silica morphologies, it has now proven possible to gain command over the thickness and channel texture of mesoporous silica films grown at the air–water interface.

The converging evidence from PXRD, TEM, and nitrogen isotherm measurements for thick mesoporous silica films shows that they have oriented and hexagonally close-packed mesopores with the channel *c*-axis aligned parallel to the growth interface. The as-synthesized and calcined films showed only (100) and (200) diffraction peaks, while additional (110) and (210) diffraction peaks can be observed for the ground samples, Fig. 3. This establishes that the mesoporous silica films are hexagonal and oriented with the channels parallel to the growth surface. TEM images of these films also define the hexagonal mesopore arrangement and orientation of the channels for as-synthesized and calcined samples. The order of the mesopores in the front and back surfaces of the film are comparable. Although the film mesostructure was maintained in all the preparations of this study, the lower degree of polymerization–condensation of the silica in the thick films that are formed at lower acidity, evidenced by the larger $(Q_2+Q_3)/Q_4$ ratio, may be the cause of the lower thermal stability compared to the thin films formed at higher acidity. Consistent with this proposal is the observed large contraction of the diameter of the mesopores for the calcined film samples. Thermal vacuum dehydration prior to calcination helps stabilize the mesostructure, Fig. 4.

Although the formation of mesoporous silica films involves silicification of a lyotropic liquid crystal, the observed POM texture of the film does not arise from organized surfactant assemblies in the channels. To amplify, the DSC trace of as-synthesized mesoporous silica films show no thermal events that can be associated with crystal–liquid crystal or isotropic melting transitions of an imbibed surfactant liquid crystal up to 250 °C, Fig. 6. Also, the fan-type texture is retained essentially invariant on removing the surfactant and after annealing the film at 450 °C, Fig. 2(C). Therefore the optical birefringence of the film does not require the surfactant to be present in the channels. Furthermore, strain anisotropy in the film is not the source of the fan-type texture. Finally, the PXRD and ^{29}Si MAS NMR data show that the silica walls of the channels are glassy. One may safely conclude that the birefringence is associated with the optically uniaxial nature of the oriented hexagonal mesoporous silica film.

The thick mesoporous silica films display two dominant morphologies which give rise to distinct POM birefringence patterns. The free-standing films synthesized with a stirring period of 3 to 5 minutes at low stirring rate, Fig. 2(A), have a structure based upon discrete morphologies which appear to have coalesced and show concentric birefringence patterns. Such morphologies have previously been observed for mesoporous silica films grown on gold[31] and glass[32] surfaces. Similar morphologies can be found in bulk preparations that yield discoid shape mesoporous silica where the channels run concentrically and coaxially around the main rotation axis of the discoid.[33] These discrete types of POM patterns presumably arise from $+2\pi$ disclinations with the rotation axes normal to the director field. Defect textures of this genre may reflect the seeds that spontaneously emerge in a lyotropic discotic hexagonal phase and originate from vertical disclinations.[13] Mesoporous silica films of this type tend to have domain structures and varied thickness. By contrast, free-standing films with a continuous and fan-type texture were obtained from a synthesis mixture with a stirring time of about 10 minutes at low stirring rate, Fig. 2(B). The film shows good homogeneity and a smoother surface compared to those formed with less of a mixing period. Films with continuous and fan-type texture can also be obtained from a synthesis mixture with a stirring time of about 5 minutes at high stirring rate. The fan textures, however, did not transform into discrete textures on changing the vessel geometry, such as its shape and size. Thus, the difference in the POM birefingence patterns and surface morphologies might be best viewed as arising from a 'switch' in the mode of formation of the free-standing film from one initiated by silicate liquid crystal seeds at the air–water interface, involving local growth and coalescence, to one involving the formation of a continuous silicate liquid crystal surface film. In both instances, silicification captures the defect structure and pattern of director fields in the precursor silicate mesophase, which is manifest in the channel design of the resulting mesoporous silica film. Boundary walls between the defect domain structures are visible in the POM images. Notwithstanding this, the birefringence textures observed for both kinds of free-standing mesoporous silica films show that the channel architecture is a silicified replica of the defect induced pattern of director fields in a silicate liquid crystal precursor. It is also noteworthy that the texture traverses the entire extent of the film implying that the mesoporosity is not confined to small domains.

It is pertinent to inquire into the relation between the optical birefringence patterns of mesoporous silica films comprised of discrete ribbon and discoid morphologies and those with fan-type textures. Recall that the channels that run down the length of the ribbon are found to whirl around the unique rotation axis of the discoids.[8,15] When these discrete morphologies are viewed orthogonal to the channel director, optical extinction is found to occur only when the channel axis coincides with the optic axes of the polarizer or analyzer. In the case of the discoids, a roughly symmetrical black cross (the isogyre) emerges from a $+2\pi$ disclination defect, while for the ribbon-shaped morphologies, a $+\pi$ disclination defect

leads to the observed textures. The observed birefringence patterns are therefore optical manifestations of the differences in the channel structures of the mesoporous silica films that are prepared by stirring the synthesis mixture for different times prior to film growth in the quiescent state. As the stirring time or rate and presumably the homogeneity of the synthesis mixture are increased, the discrete birefringence pattern of the films so formed gradually merge into ones displaying the continuous fan-type texture. This behavior might be thought as a 'switch' in the mode of formation of the films at the air–water interface, from one primarily involving the polymerization, growth and coalescence of a population of silicate liquid seeds to one based on the polymerization and thickening of a continuous silicate liquid crystal film.

The liquid crystal POM patterns and surface morphologies not only depend on the synthesis conditions, they also change with the substrate properties. This can be seen from POM images for films grown on amorphous surfaces, such as glass plates or tubes and the atomically flat mica surface. It is interesting to note that the POM patterns for the films grown on mica differ from those on the other surfaces or subphases. Discrete and fan-type textures are replaced by extensive areas of dark, grey and light patches, Fig. 10. The patterns of parallel striations within the different patches of the mesoporous silica film meet at angles of 60 or 120°. This observation suggests that growth of the hexagonal mesoporous silica film occurs with the channel axis preferentially aligned along the hexagonal *a*,*b*-axes of the mica (001) surface.

Finally, the observation of liquid crystal textures in mesoporous silica films grown at the air–water interface under dilute aqueous and acidic conditions provides direct evidence for a templating pathway based upon cooperative assembly and organization of silicate micellar species[4,5,16–18] rather than a pre-formed silicate liquid crystal.[21]

Conclusions

Optical birefringence patterns observed for free-standing mesoporous silica films are shown to originate from mesoscale optical anisotropy associated with the polarization response of electron density circumscribing a hexagonal array of glassy silica channels. The existence of the birefringence shows that the channel architecture is a silicified replica of the defect induced pattern of director fields in a silicate liquid crystal precursor. Alteration of synthesis conditions, mixing and substrates enables control over the film texture, which reflects changes in channel structure arising from the operation of distinct film growth processes. The ability to synthesize 5–10 μm thick mesoporous silica films and tailor their channel architecture can be considered to represent a significant step towards the practical realization of mesoporous silica thin film-based devices and technologies.

Financial support from Mobil Technology Company is deeply appreciated. H.Y. is grateful for an Ontario Graduate Scholarship held during this research period. We also thank Mr. G. Vovk for setting up the McBain balance and for valuable discussions on data analysis, and Dr. P. Aroca for assistance with the recording of solid state NMR spectra.

References

1 K. Hiltrop, *Lyotropic Liquid Crystals*, in *Liquid Crystals*, ed. H. Stegemeyer, Steinkopff Darmstadt, Springer, Germany, 1994, pp. 143–171.
2 D. Demus and L. Richter, *Textures of Liquid Crystals*, Verlag Chemie, Weinheim, Germany, 1978.
3 N. H. Hartshorne, *The Microscopy of Liquid Crystals*, Microscope Publications Ltd., London, 1974, pp. 104–138.
4 (*a*) C. T. Kresge, M. Leonowicz, W. J. Roth, J. C. Vartuli and J. C. Beck, *Nature* (*London*), 1992, **359**, 710; (*b*) J. S. Beck, J. C. Vartuli, W. J. Roth, M. E. Leonowicz, C. T. Kresge, K. D. Schmitt, C. T.-W. Chu, D. H. Olson, E. W. Sheppard, S. B. McCullen, J. B. Higgins and J. L. Schlenker, *J. Am. Chem. Soc*., 1992, **114**, 10 834.
5 Q. Huo, D. I. Margolese, U. Clesia, P. Feng, T. E. Gler, P. Sieger, R. Leon, P. M. Petroff, F. Schüth and G. D. Stucky, *Nature* (*London*), 1994, **368**, 317.
6 H. Yang, N. Coombs, I. Sokolov and G. A. Ozin, *Nature* (*London*), 1996, **381**, 589.
7 H. Yang, N. Coombs, Ö. Dag, I. Sokolov and G. A. Ozin, *J. Mater. Chem*., 1997, **7**, 1755.
8 N. Coombs, D. Khushalani, G. A. Ozin, S. Oliver, G. C. Shen, I. Sokolov and H. Yang, *J. Chem. Soc*., *Dalton Trans*., 1997, 3941.
9 (*a*) I. A. Aksay, M. Trau, S. Manne, I. Honma, N. Yao, L. Zhou, P. Fenter, P. M. Eisenberger and S. M. Gruner, *Science*, 1996, **273**, 892; (*b*) A. S. Brown, S. A. Holt, T. Dam, M. Trau and J. W. White, *Langmuir*, 1997, **13**, 6363.
10 S. H. Tolbert, T. E. Schäffer, J. Feng, P. K. Hansma and G. D. Stucky, *Chem. Mater*., 1997, **9**, 1962.
11 J. Feng, Q. Huo, P. M. Petroff and G. D. Stucky, *Appl. Phys. Lett*., 1997, **71**, 620.
12 Y. Bouligand, *J. Phys*., 1980, **41**, 1297.
13 Y. Bouligand, *J. Phys*., 1980, **41**, 1307.
14 M. Kléman, *Points, Lines and Walls: In Liquid Crystals, Magnetic Systems and Various Ordered Media*, John Wiley & Sons Ltd., Chichester, 1983.
15 H. Yang, N. Coombs and G. A. Ozin, *Nature* (*London*), 1997, **386**, 692.
16 A. Monnier, F. Schuth, Q. Huo, D. Kumar, D. Margolese, R. S. Maxwell, G. D. Stucky, M. Krishnamurty, P. Petroff, A. Firouzi, M. Janicke and B. F. Chmelka, *Science*, 1993, **261**, 1299.
17 (*a*) A. Firouzi, F. Atef, A. G. Oertli, G. D. Stucky and B. F. Chmelka, *J. Am. Chem. Soc*., 1997, **119**, 3596; (*b*) A. Firouzi, D. Kumar, L. M. Bull, T. Sieger, Q. Huo, S. A. Walker, J. A. Zasadzinski, C. Glinka, J. Nicol, D. I. Margolese, G. D. Stucky and B. F. Chmelka, *Science*, 1995, **267**, 1138.
18 (*a*) C.-Y. Chen, H.-X. Li and M. E. Davis, *Microporous Mater*., 1993, **2**, 17; (*b*) C.-Y. Chen, S. L. Burkett, H.-X. Li and M. E. Davis, *Microporous Mater*., 1993, **2**, 27.
19 P. T. Tanev and T. J. Pinnavaia, *Science*, 1995, **267**, 865.
20 D. M. Antonelli and J. Y. Ying, *Angew. Chem., Int. Ed. Engl*., 1995, **34**, 2014.
21 (*a*) G. S. Attard, J. C. Glyde and C. G. Göltner, *Nature* (*London*), 1995, **378**, 366; (*b*) M. Antonietti and C. Goltner, *Angew. Chem., Int. Ed. Engl*., 1997, **36**, 910.
22 P. Behrens, *Angew. Chem., Int. Ed. Engl*., 1996, **35**, 515.
23 H. Yang, G. Vovk, N. Coombs, I. Sokolov and G. A. Ozin, *J. Mater. Chem*., 1998, **8**, 743.
24 T. Tasumi, K. Koyano, Y. Tanaka and S. Nakata, *Chem. Lett*., 1997, 469.
25 (*a*) S. J. Gregg and K. S. W. Sing, *Adsorption, Surface Area and Porosity*, Academic Press, London, 2nd edn., 1982; (*b*) H. Naono, M. Hakuman and T. Shiono, *J. Colloid Interface Sci*., 1997, **186**, 360; (*c*) M. J. Meziani, J. Zajac, D. J. Jones, J. Rozière and S. Partyka, *Langmuir*, 1997, **13**, 5409; (*d*) M. Kruk, M. Jaroniec and A. Sayari, *Langmuir*, 1997, **13**, 6267.
26 H. Yang, A. Kuperman, N. Coombs, S. Mamiche-Afara and G. A. Ozin, *Nature* (*London*), 1996, **379**, 703.
27 O. Regev, *Langmuir*, 1996, **12**, 4940.
28 Y. S. Lee, D. Surjadi and J. F. Rathman, *Langmuir*, 1996, **12**, 6202.
29 J. Böcker, M. Schlenkrich, P. Bopp and J. Brickmann, *J. Phys. Chem*., 1992, **96**, 9915.
30 J. R. Lu, Z. X. Li, J. Smallwood, R. K. Thomas and J. Penfold, *J. Phys. Chem*.. 1995, **99**, 8233.
31 H. Yang, N. Coombs and G. A. Ozin, *Adv. Mater*., 1997, **8**, 811.
32 (*a*) H. W. Hillhouse, T. Okubo, J. W. van Egmond and M. Tsapatsis, *Chem. Mater*., 1997, **9**, 1505; (*b*) A. Kuperman, S. Mamiche-Afara, G. A. Ozin and H. Yang, *Technical Report to Mobil Technology Company*, June 1995.
33 G. A. Ozin, H. Yang, I. Sokolov and N. Coombs, *Adv. Mater*., 1997, **8**, 662.

Paper 8/00004B; *Received* 2*nd January*, 1998